Full Paper
doi.org/10.1002/chem.202000204

Photochemistry

Enhanced Photocatalytic Hydrogen Production by Hybrid Streptavidin-Diiron Catalysts

Anindya Roy,[a, b] Michael D. Vaughn,[a] John Tomlin,[a] Garrett J. Booher,[a] Gerdenis Kodis,[a] Chad R. Simmons,[a] James P. Allen,[a] and Giovanna Ghirlanda*[a]

Abstract: Hybrid protein–organometallic catalysts are being explored for selective catalysis of a number of reactions, because they utilize the complementary strengths of proteins and of organometallic complex. Herein, we present an artificial hydrogenase, StrepH2, built by incorporating a biotinylated [Fe–Fe] hydrogenase organometallic mimic within streptavidin. This strategy takes advantage of the remarkable strength and specificity of biotin-streptavidin recognition, which drives quantitative incorporation of the biotinylated diironhexacarbonyl center into streptavidin, as confirmed by UV/Vis spectroscopy and X-ray crystallography. FTIR spectra of StrepH2 show characteristic peaks at shift values indicative of interactions between the catalyst and the protein scaffold. StrepH2 catalyzes proton reduction to hydrogen in aqueous media during photo- and electrocatalysis. Under photocatalytic conditions, the protein-embedded catalyst shows enhanced efficiency and prolonged activity compared to the isolated catalyst. Transient absorption spectroscopy data suggest a mechanism for the observed increase in activity underpinned by an observed longer lifetime for the catalytic species $Fe^{I}Fe^{0}$ when incorporated within streptavidin compared to the biotinylated catalyst in solution.

Introduction

Hydrogen metabolism is regulated by hydrogenases, a class of metalloenzymes that catalyze reduction of protons as well as hydrogen oxidation under mild conditions at near-thermodynamic potential, using bimetallic centers (either [Fe–Fe] or [Ni–Fe]) at the active site.[1,2] Of these, the [Fe–Fe] hydrogenases are the most efficient for hydrogen production.[3] They incorporate an unusual diiron organometallic complex coordinated by a azadithiolate bridging ligand, carbon monoxide, and cyanide ligands, tethered via a single cysteine to a cubane-type [4Fe–4S] cluster to form the H-cluster.[1] The diiron cluster, inactive in isolation, is stabilized and activated via second-sphere interactions when incorporated within the protein.[4–6] The apo hydrogenase also accepts synthetic, non-native cofactors, such as a propanedithiolate bridging ligand, resulting in negligible residual activity compared to WT hydrogenase, further indicating the role of the protein environment.[7–11] Bioinspired structural organometallic mimics of [Fe–Fe] hydrogenases built around a bridging dithiolate ligand have been extensively explored, providing a rich repertoire of chemical structures. These models serve as an important testing ground to assess the features that impart catalytic prowess to the H-cluster.[12–24] While most are soluble in organic solvent, several examples of complexes built on a $(\mu\text{-S-}(CH_2)_3\text{-S})[Fe_2(CO)_6]$ scaffold and modified with polar groups to facilitate derivatization and/or attachment have been reported.[12–16] Compared to the hydrogenases, these models show moderate catalytic activity, and generally are inefficient catalysts in photoinduced hydrogen production in part because they degrade during long irradiation, often resulting in the loss of the CO ligands.[17–25] Simple diiron-dithiolate complexes have also been encased within biopolymers or non-biological scaffolds, such as cyclodextrins, surfactants, dendrimers, or metal-organic frameworks (MOFs), showing that supramolecular confinement enhances photoinduced hydrogen production.[20,26–29] However, these systems cannot provide the tailored second-sphere interactions that in natural hydrogenases activate the organometallic center by stabilization of the catalytically active conformation.[8,30,31]

In a quest for robust, minimalist artificial hydrogenases, our group and others have incorporated these organometallic centers into peptides and proteins using distinct strategies.[32–36] Promising results in photocatalyzed hydrogen production were obtained by anchoring diiron hexacarbonyl complexes to a helical peptide or within Cyt c by exploiting the thiol moiety of cysteine in CXXC motifs,[32,34] or using an artificial amino acid to tether the diiron hexacarbonyl complex to a helical complex.[35] Encapsulation of organometallic catalysts within host proteins yielded mixed results: No improvements were ob-

[a] Dr. A. Roy, Dr. M. D. Vaughn, Dr. J. Tomlin, G. J. Booher, Dr. G. Kodis, C. R. Simmons, Prof. J. P. Allen, Prof. G. Ghirlanda
School of Molecular Sciences, Arizona State University
Tempe, AZ 85287-1604 (USA)
E-mail: gghirlanda@asu.edu

[b] Dr. A. Roy
Present Address: Molecular Engineering and Sciences
Institute for Protein Design, University of Washington
Seattle, WA 98195-1655 (USA)

Supporting information and the ORCID identification number(s) for the author(s) of this article can be found under: https://doi.org/10.1002/chem.202000204. It contains experimental protocols, NMR spectra, electrochemical data, transient absorption data, and HRMS.

served when incorporating diiron hexacarbonyl complexes in nitrobindin.[37] A synthetically convenient strategy to build hybrid metalloproteins is based on the streptavidin-avidin complex; since its introduction,[38] this strategy has been successfully used to catalyze enantioselective reduction of a variety of organic substrates, indicating that catalysts linked to biotin interact with the protein.[39–44] In this system, cobalt catalysts for hydrogen production retained or improved catalytic activity, especially when probed at high pH.[45,46] Mutations close to the organometallic complex improved pH dependence and initial rates/TON as compared to the naked catalyst.[46]

Inspired by these results, we utilized the streptavidin-avidin system to stably encapsulate a biomimetic diiron hexacarbonyl complex, reasoning that the biotin scaffold could stabilize its catalytically active state, in analogy to what observed in natural [FeFe] hydrogenases.[30]

Building on the extensive literature on this class of compounds, summarized above, we chose a simple organometallic diiron hexacarbonyl center functionalized with a hydroxyl moiety, and tethered it to biotin; reconstitution with streptavidin generated an artificial hydrogenase, StrepH2. The biotinylated hydrogenase mimic is readily incorporated into streptavidin and displayed spectroscopic features typical of intact diiron hexacarbonyl centers. StrepH2 catalyzes hydrogen production under photocatalytic conditions with enhanced efficiency compared to the isolated diiron hexacarbonyl center. The crystal structure of StrepH2 provides a blueprint for the design of improved versions by selective mutation of residues in contact within the active site.

Results and Discussion

Synthesis and characterization of the biotinylated-[Fe–Fe] hydrogenase mimic

The biotinylated [Fe–Fe] hydrogenase mimic (referred to as BiotH2 or **3** herein) was obtained as described in Scheme 1 by coupling **2** to biotin in the presence of HATU with high yield. Compound **2** was synthesized following established procedures.[47–49] Briefly, the synthesis of **2** started from 3-mercapto-2-(mercaptomethyl)propan-1-ol (**1**),[50] followed by refluxing with $Fe_3(CO)_{12}$ in toluene to yield the metallic complex.[47,48]

BiotH2 was then incorporated into streptavidin to form the complex StrepH2. The stoichiometry of binding was assessed by a displacement assay using 2-(4′-hydroxyazobenzene)benzoic acid (HABA) (Supporting Information). In solution, streptavidin exists as a tetramer formed by units parallel to each other in pairs, with the biotin cavity oriented accordingly (two „up" and two „down") in the assembly. We found that the stoichiometry of binding for BiotH2 to streptavidin is approximately 0.7:1 (expressed as BiotH2 to streptavidin monomer), similar to values reported for the biotin-streptavidin system,[39–41] and indicating that introduction of the diiron-hexacarbonyl moiety at the valeric chain of biotin is well tolerated.

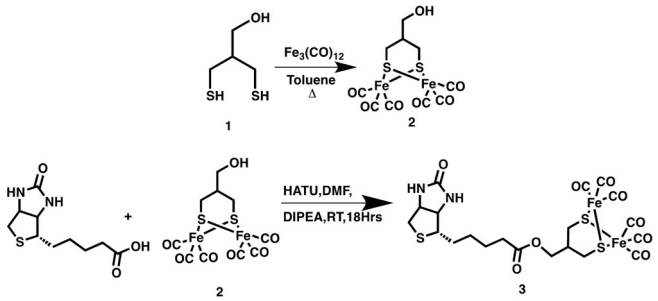

Scheme 1. Synthesis of BiotH2.

The structural integrity of the diironhexacarbonyl moiety of **3** in StrepH2 was verified by UV/Vis and FTIR spectroscopy. Purified StrepH2 assembly showed two distinct bands in the UV/Vis spectrum, centered around 329 nm and 474 nm. These features are characteristic of Fe_2S_2 butterfly complexes and consistent with the reported literature for similar organometallic complexes (Figure 1, Panel 1).[32,36] Possible changes to the environment surrounding the organometallic cluster upon incorporation into streptavidin were assessed by FTIR spectroscopy, which reports on the environment of the CO groups via changes to the C=O stretching modes. To interpret the FTIR spectra, we used as benchmark the changes observed for the 1,3 propane-dithiolate diiron-hexacarbonyl complex as a function of solvent polarity.[51,52] In nonpolar solvents, a total of five stretching frequencies were observed, reflecting a pseudo C_{2v} symmetry. In polar solvents, three of these low frequency bands collapse to give rise to one broad absorption band.[51,52]

We compared the thin film FTIR signatures of BiotH2 with those of StrepH2, and found evidence of increased hydrophobic interactions in StrepH2. FTIR spectra of BiotH2 showed two sharp peaks at 2073 and 2030 cm^{-1}, and a broad absorption band at 1990 cm^{-1}, consistent with related organometallic analogues in polar solvents, and were assigned to the coupled stretching frequency of -CO (Figure 2, Panel 2).[51] In StrepH2, the two sharp peaks were shifted to 2074 and 2034 cm^{-1}, while the broad absorption feature showed three distinct shoulders (2001, 1991, 1971 cm^{-1}) implying a change in the environment of the organometallic cluster after binding to streptavidin. The splitting of the low wavenumber absorption band into three bands indicated a change in polarity around the CO groups to a more hydrophobic environment upon binding to the protein scaffold compared to the naked catalyst in solution.[52]

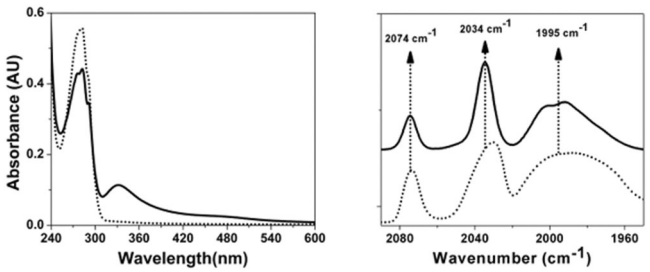

Figure 1. UV/Vis and FTIR spectra. StrepH2 panel 1: UV/Vis spectra of streptavidin (black, dotted) and StrepH2 (black, solid). Panel 2: FTIR spectra of BiotH2 in the absence (dotted line, bottom trace) and presence (solid, top trace) of streptavidin.

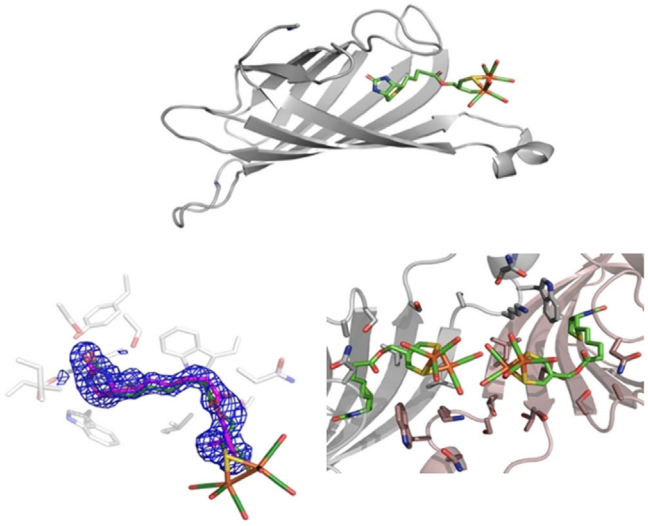

Figure 2. X-ray structure of StrepH2 showing BiotH2 incorporated in the streptavidin pocket (left panel). The $2F_o-F_c$ electron density reveals the binding pocket used to build the BiotH2 bound model (middle panel), and the arrangement of two adjacent streptavidin monomers with ligand interactions of neighboring substituents are shown (right panel).

Structure of StrepH2

The X-ray crystal structure of StrepH2 was determined to a resolution of 2.05 Å confirming placement of the ligand into the protein pocket (Figure 2, PDB ID 5VCQ). The structure was solved by molecular replacement, using PDB 1MK5 as the search model (see SI for details). The residual *Fo-Fc* difference electron density in the binding pocket of was further examined to assess ligand occupancy. The $2F_o-F_c$ map revealed a well resolved structure for the portion containing the biotin cofactor, including the valeric chain and the 2-methyl-propanol portion, while the area corresponding to the diiron hexacarbonyl site was not resolved in the experimental density. Partial occupancy of biotinylated ligands in the streptavidin pocket is observed in all reported X-ray structures, because the protein monomers arrange so that ligands incorporated within the protein cavity abut onto one another causing steric clashes and preventing full occupancy.[41] To gain further insights on the environment of the complex in the protein, the remaining portion of the ligand was modeled in Rosetta (see Supporting Information) using the crystal structure of 1,3-propanedithiol in complexed with diiron hexacarbonyl as starting point (CSDS accession file AQIQIB).

An analysis of the binding pocket with the ligand reconstituted as described shows that the diiron hexacarbonyl complex is accommodated in the streptavidin pocket, and is surrounded by protein loops on three sides, with the fourth side facing a second streptavidin unit. The diiron hexacarbonyl portion is partly exposed to the solvent, thus facilitating exchange of protons and electrons. While we did not observe direct contacts with any of the side chains or backbone amide moieties, the complex is close enough for interaction with several residues, in particular we note possible interactions with Lys 106 from the neighboring monomer.

Catalytic activity of StrepH2

We used cyclic voltammetry to analyze the electrochemical properties of BiotH2 in the presence and absence of streptavidin; experiments were carried out at 10 μM catalyst concentration, which ensures complete solubility of the complex (Supplementary Information). Cyclic voltammograms of BiotH2 at pH 6.0 showed an irreversible reductive peak at −980 mV vs. SHE, corresponding to $Fe^{I}Fe^{I}/Fe^{I}Fe^{0}$ reduction consistent with other water soluble [Fe-Fe] hydrogenase mimics.[35,53,54] When the pH of the solution was lowered to 4.5, an increase in a reductive wave corresponding to proton reduction was observed (Figure 3, left panel). Controls were carried out at low pH to confirm the catalytic current was not due to proton reduction with a bare electrode at negative potential (Supplementary Information). Direct electrochemistry of StrepH2 assembled in situ by addition of 15 μM of streptavidin to a 10 μM solution of BiotH2 at pH 6.0 resulted in a significant decrease of the reductive current, most likely due to the encapsulation of the complex within streptavidin (SI). To address this issue, we performed protein film voltammetry (PFV), to ensure rapid electron transfer with the electrode.

Because streptavidin has a pI of approximately 5–6, interaction with the negatively charged electrode surface might have been more favorable at low pH, resulting in conditions appropriate for PFV. Cyclic voltammetry experiments on StrepH2 immobilized on a glassy carbon electrode showed a reductive current that corresponded to $Fe^{I}Fe^{I}/Fe^{I}Fe^{0}$ reduction at pH 6 (Figure 3, right panel). When the pH was lowered to 4.5, the reductive transition became catalytic, indicating proton reduction. Controls with streptavidin films (in the absence of BiotH2) showed no redox activity in the range examined, indicating that the catalytic process is due to the protein-organometallic complex on the electrode.

We investigated the ability of StrepH2 to catalyze hydrogen production under photocatalytic conditions by measuring the catalytic efficiency of BiotH2 and StrepH2. In general, diiron hexacarbonyl complexes are inefficient catalysts in photoinduced hydrogen production because they degrade during long irradiation, often resulting in the loss of the CO ligands.[17–25] However, the streptavidin scaffold could provide shielding via specific interactions with the catalyst. In this assay, the catalyst at 5.14 μM concentration in the presence of

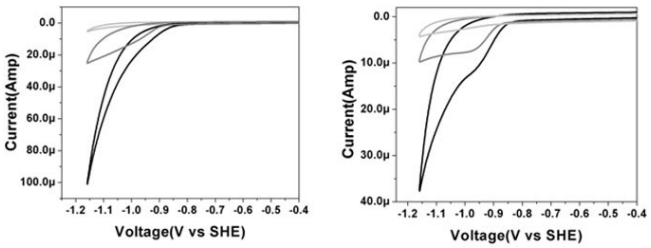

Figure 3. Cyclic voltammetry. Left: Cyclic voltammetry traces of BiotH2 at pH 4.5 (black), pH 6.0 (gray) and StrepH2 at pH 6.0 (light gray) in solution. Right: Protein film voltammetry of StrepH2 at pH 4.5 (black), pH 6.0 (gray) and streptavidin at pH 4.5 (light gray).

150 μM $[Ru(bpy)_3]^{2+}$ as a photosensitizer and 100 mM ascorbic acid as a sacrificial electron donor at pH 4.5 was irradiated by light, allowing for the amount of hydrogen evolved upon irradiation to be monitored over time by GC (see the Supporting Information).

We found that BiotH2 gives rise to a TON of 6.42(±0.05). The naked catalyst was deactivated approximately after 3 hours under continuous irradiation. Under the same conditions, StrepH2 resulted in a TON of 47.63(±3.16) over 11 hours. While the initial rate of production is comparable for the two species, the net increase in TON appears to derive, in large part, from a much longer lifetime of the catalyst when embedded in the protein (Figure 4): while the activity of BiotH2 starts to level off after approximately 100 minutes, StrepH2 continues to produce hydrogen for at least 9 hours.

Previous work incorporating a similar $(\mu\text{-S-}(CH_2)_3\text{-S})[Fe_2(CO)_6]$ complex into nitrobindin showed no improvement in activity when compared to the isolated synthetic catalyst, and much slower initial rates, attributed by the authors to decreased accessibility of the ruthenium photosensitizer to the diiron active site. The activity for the nitrobindin complex leveled off after approximately 2 hours.[37] Our results, however, show a marked increase in activity, and point to an effect due in large part to protection of the catalyst from inactivation.

To verify this hypothesis, we interrogated the system by transient absorption spectroscopy. This technique allows for the elucidation of the electron transfer mechanism in photocatalyzed systems by comparing the behavior of BiotH2 (**3**) and StrepH2. Experiments were carried out in conditions mirroring closely those used for the hydrogen production studies (vide supra), in the presence of ascorbic acid as a sacrificial electron donor and $[Ru(bpy)_3]^{2+}$ as a photosensitizer, upon excitation at 480 nm. The evolution-associated-difference spectra (EADS) of BiotH2 and StrepH2 obtained after global analysis of the data measured in the 9 ms delay time window are shown in Figure 5. Each EADS has an associated lifetime and shows spectral features characteristic of the transient species involved

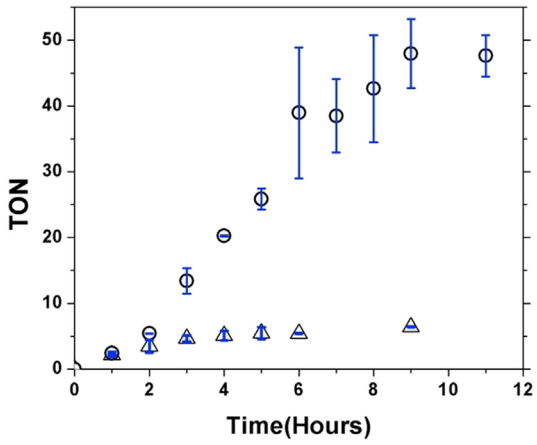

Figure 4. Visible light-driven hydrogen production by StrepH2 (5.14 μM) (open circles) and by BiotH2 (5.14 μM) (solid circles) in the presence of 150 μM $[Ru(bpy)_3]^{2+}$ and 100 mM ascorbate buffer at pH 4.5. Samples were irradiated with visible light (410–770 nm).

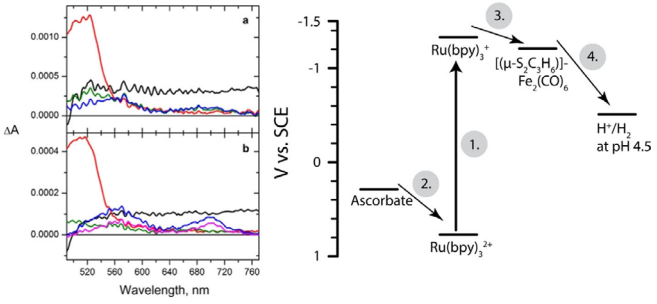

Figure 5. Left panel: Evolution-associated-difference spectra (EADS) obtained after global analysis of the transient absorption data for BiotH2 and StrepH2 in presence of $[Ru(Bpy)_3]^{2+}$ as a photosensitizer and ascorbic acid as a sacrificial electron donor upon excitation at 480 nm in argon degassed ascorbate buffer at pH 4.5 and 45% (v/v) DMSO solution. (a) EADS for BiotH2: lifetimes 17 ns (black), 10 μs (green), 51 μs (red) and 486 μs (blue). (b) EADS for StrepH2 system: lifetimes 50 ns (black), 61 μs (red), 823 μs (green), 2.39 ms (blue) and nondecaying in 9 ms time delay window component (magenta). Right panel: Schematic proposed electron transfer mechanism in the photocatalytic hydrogen production system.

in the photoinduced electron transfer reaction as depicted in Figure 5 (right panel). Transient absorption data for BiotH2 were satisfactorily fitted with 4 lifetimes: 17 ns, 10 μs, 51 μs and 486 μs. The EADS corresponding to the species with a 17 ns lifetime shows broad induced absorption at 500–800 nm and ground state bleaching at 450 nm characteristic of the $[Ru(Bpy)_3]^{2+}$ excited state.[27] This state decays via an electron transfer from the ascorbic acid to form the transient $[Ru(Bpy)_3]^{+}$ species, which has a characteristic strong induced absorption at 520 nm.[55] The transient $[Ru(Bpy)_3]^{+}$ (see 51 μs EADS) consequently decays in 51 μs via secondary electron transfer and give rise to the $Fe^{I}Fe^{0}$ species, with a lifetime of 486 μs and characteristic induced absorption at 570 nm and 700 nm.[55] The minor EADS associated with a lifetime of 10 μs corresponds to the $[Ru(Bpy)_3]^{+}$ species which are quenched by some other means and is not involved in the electron transfer to $Fe^{I}Fe^{I}$. There was no transient absorption signal at time delays longer than 1 ms (see Supporting Information for more transient absorption data). In contrast, transient absorption data for the StrepH2 system were satisfactorily fitted with 5 lifetimes: 50 ns, 61 μs, 823 μs, 2.39 ms and a nondecaying component. Similarly to the BiotH2 case, the EADS with lifetimes of 50 ns and 61 μs can be attributed to the $[Ru(Bpy)_3]^{2+}$ excited state and transient $[Ru(Bpy)_3]^{+}$, respectively. The lifetime of the $Fe^{I}Fe^{0}$ species can be fitted with two time constants, one with 2.39 ms and a nondecaying component (see the 2.39 ms EADS and constant EADS), suggesting complex interaction and multiple decay pathways in the protein environment. The 823 μs EADS displays characteristic induced absorption at around 500 nm and is most likely associated with the oxidized and/or reduced streptavidin species: identical transient was observed in the control experiment with apo streptavidin (see Supporting Information).[56–58] Incorporation of BiotH2 into streptavidin thus resulted in an extended (more than 4 times) lifetime for the catalytically active form of the catalyst, with $Fe^{I}Fe^{0}$ oxidation state, from 486 μs to 2.39 ms. The $Fe^{I}Fe^{0}$ is the first inter-

mediate in hydrogen evolution by diiron hexacarbonyl complexes, as summarized in Figure 5 (right panel).

Conclusions

Here, we have demonstrated that incorporation of a biotinylated hydrogenase mimic into streptavidin results in increased activity compared to the bare catalyst. Streptavidin-based catalysts that interface an organometallic complex with a protein scaffold have been used successfully in particular to impart stereospecificity to a reaction.[38,41,42,59–62] This approach, however, had been partially successful in the catalysis of proton reduction: incorporation of cobalt catalysts did not enhance activity at neutral pH, although significant effects were observed at high pH when using $[Ir(bpy)(ppy)_2]PF_6$ as photosensitizer and triethanolamine as sacrificial electron donor; these conditions require the use of acetonitrile as co-solvent.[45,46] Herein, we chose to explore the incorporation of a different type of hydrogen evolving complex, a biomimetic diiron hexacarbonyl active center. Hydrogenase mimics based on the diironhexacarbonyl moiety present low activity and are generally unstable. We found that photocatalytic activity expressed as TON for StrepH2 is about $\approx$8 times higher than for the biotinylated complex BiotH2. The increase in TON is largely due to increased lifetime of the catalytically competent intermediate form of the diiron hexacarbonyl complex, $Fe^{I}Fe^{0}$, in the case of StrepH2 but not of BiotH2, as demonstrated by transient spectroscopy. The origins of this increase in lifetime are not entirely clear. It is possible that interactions of the complex with nearby residues serve to stabilize the reduced form, and prevent possible side reactions, in analogy with what observed upon incorporation of diiron hexacarbonyl complexes in MOFs[26] In addition, the proximity of Lys106 may provide a proton relay that facilitates generation of molecular hydrogen. The crystal structure of StrepH2 provides information for further optimization of the system by engineering mutations in proximity to the iron-sulfur complex. Such mutations could increase activity for example by providing a proton relay during the catalytic cycle, or by stabilizing the relevant redox state of the metal center.[63–67] Finally, we note that the streptavidin scaffold provides a robust environment, which is stable upon immobilization on electrodes. This feature may provide additional avenues for exploring light-aided electrocatalysis.

Experimental Section

Synthesis of 3

Compound **3** (BiotH) was synthesized by coupling D-Biotin and 2 in DMF using HATU as coupling auxiliary. 180.56 mg (0.74 mmol) of biotin, 308 mg (0.74 mmol) of compound 3, and 281.37 mg (0.74 mmol) of HATU were dissolved in 6 mL of anhydrous DMF and 185.22 mg of dry DIPEA was added to the mixture. The resulting mixture was stirred under an inert atmosphere overnight, and DMF was evaporated under reduced pressure; the yellowish red crude oil was purified on a silica gel column using 10% MeOH in DCM (RF: 0.65). ^{1}H NMR (DMSO, δ [ppm]): 1.19–1.67 (m, 9H), 2.28–2.34 (m, 2H), 2.59 (d, 1H), 2.77 (dd, 2H), 3.09 (m, 1H), 3.62 (m, 2H), 3.81 (d, 1H), 4.11 (m, 1H), 4.30 (t, 1H), 6.35 (s, 1H), 6.41 (s, 1H). ^{13}C NMR (DMSO, δ [ppm]): 24.82, 28.42, 33.61, 33.92, 41.29, 43.20, 55.78, 59.62, 61.48, 63.43, 66.75, 163.14, 172.96, 208.41. Mass: Calculated (M^+) 641.92. Obtained 642.92.

Electrochemistry

All electrochemical studies were performed on a CH-Instruments model 1242B electrochemical workstation using a SCE reference electrode, a Pt-mesh counter electrode and a glassy carbon electrode (3 mm diameter) in a Coy anaerobic chamber. Cyclic Voltammetry scans were performed in 100 mM acetate, 50 mM NaCl buffer of desired pH (4.5 and 6.0) at 100 mV s^{-1} scan rate. Working electrode was cleaned in between different samples and a blank was recorded to ensure cleanliness of the electrode. For protein film voltammetry, 1 μL of 100 μM catalyst was placed directly on the active electrode surface and dried under vacuum. This electrode was then placed into fresh buffer of different pH and CVs were recorded.

Photoinduced hydrogen production

Photocatalytic hydrogen was monitored by quantifying the evolved hydrogen gas by gas-chromatography. For these experiments, solutions containing 150 μM $Ru(Bpy)_3^{2+}$, 100 mM ascorbate pH 4.5 and the catalyst at desired concentration were placed in a custom made gas tight cuvette (0.1 cm pathlength), and degassed extensively. The cuvette was then irradiated with a white LED (Philips Luxeon S5000 part number LXS9-PW27-0041), and the light intensity at the sample was maintained at 1100 W m^{-2} for all the experiments (one sun). The amount of hydrogen evolved as a function of time was monitored by injecting 100 μL of argon, sampling 100 μL of the overhead gas with a gas tight syringe, and analyzing it on a GC (SRI instruments, Model no. 310C) using a 5 Å molecular sieve column, a thermal conductivity detector and Ar as carrier gas. The GC instrument was calibrated using a gas standard (1% H_2 and bulk N_2, Figure S2).

Transient absorption measurements

Transient absorption spectra and kinetics on the ps-ms time scale were obtained using EOS spectrometer (Ultrafast Systems). Excitation at 480 nm was from an optical parametric amplifier (Spectra Physics) pumped with laser pulses of 100 fs at 800 nm generated by an amplified, mode-locked titanium sapphire laser system (Millennia/Tsunami/Spitfire, Spectra Physics) operating at 1 kHz or 100 Hz repetition rate and allowing to utilize the 400 μs and 9 ms EOS spectrometer kinetics decay time windows, respectively. The instrument response function (IRF) was ca. 800 ps.

Crystallization of streptavidin-BiotH complex

All manipulations for crystallography were carried out in a Coy anaerobic chamber (95% N_2, 5% H_2). The complex, StrepHyd1, was crystallized using hanging drop vapor diffusion techniques. The protein-organometallic complex was obtained by mixing 27 mg mL^{-1} of streptavidin with 3 molar excess of BiotH. The resulting solution was centrifuged for 10 minutes at 10,000 g to remove any precipitated protein. The composition of the reservoir solution for successful crystallization was as follows: 100 mM TRIS pH 8.5; 200 mM $MgCl_2$; 25% PEG4000. Drops of the protein and ligand solution were mixed with an equal volume of the reservoir solution before_equilibration. Crystal growth was observed within 4–7 days. The yellow colored crystals were subsequently harvested

using cryo-loops (Hampton Research), and cryo-cooled by plunging in a liquid nitrogen bath.

Crystallographic data collection, processing, and structure solution

Crystallographic data collection was performed at the Advanced Light Source (ALS) at Lawrence Berkeley National Lab beamline 8.2.2. Diffraction data were collected on an ADSC Q315R detector at $\lambda = 1.0$ Å. $180 \times 1^{\circ}$ oscillation frames were collected and were indexed, refined, integrated, and scaled using the HKL2000 package.[68] Initial crystallographic phases were determined by molecular replacement using wild-type core streptavidin (PDB: 1MK5) as the search model. The structure was built upon a single solution, and model building and refinement were performed using PHENIX, CCP4, and COOT.[69–71] Calculations of R_{free} for each of the datasets were based upon 5% of the unique reflections, with a final model that was in very good agreement with the data with R_{work} and R_{free} of 16.5% and 21.8%. Crystallographic and refinement statistics are given in Table 1, Supporting Information. The atomic coordinates and structure factors have been deposited in the Protein Data Bank (PDB) with accession code 5VCQ. Both structures shown in Figures 1 and 3 were generated with PYMOL.

Acknowledgements

This work was supported by NSF award CHE-1508301. We thank Dr. Y. Su at the Molecular mass spectrometry facility, UCSD for HRMS analysis, and Dr. Brian Cherry for assistance with NMR data collection.

Conflict of interest

The authors declare no conflict of interest.

Keywords: catalysis · hybrid enzymes · hydrogen production · streptavidin-avidin · X-ray crystallography

[1] J. C. Fontecilla-Camps, A. Volbeda, C. Cavazza, Y. Nicolet, *Chem. Rev.* **2007**, *107*, 4273 – 4303.
[2] Y. Nicolet, C. Piras, P. Legrand, C. E. Hatchikian, J. C. Fontecilla-Camps, *Structure* **1999**, *7*, 13 – 23.
[3] M. W. W. Adams, *Biochim. Biophys. Acta* **1990**, *1020*, 115 – 145.
[4] P. Knörzer, A. Silakov, C. E. Foster, F. A. Armstrong, W. Lubitz, T. Happe, *J. Biol. Chem.* **2012**, *287*, 1489 – 1499.
[5] M. Y. Darensbourg, R. D. Bethel, *Nat. Chem.* **2012**, *4*, 11 – 13.
[6] G. Berggren, A. Adamska, C. Lambertz, T. R. Simmons, J. Esselborn, M. Atta, S. Gambarelli, J.-M. Mouesca, E. Reijerse, W. Lubitz, T. Happe, V. Artero, M. Fontecave, *Nature* **2013**, *499*, 66 – 69.
[7] J. F. Siebel, A. Adamska-Venkatesh, K. Weber, S. Rumpel, E. Reijerse, W. Lubitz, *Biochemistry* **2015**, *54*, 1474 – 1483.
[8] J. Esselborn, C. Lambertz, A. Adamska-Venkatesh, T. Simmons, G. Berggren, J. Noth, J. Siebel, A. Hemschemeier, V. Artero, E. Reijerse, M. Fontecave, W. Lubitz, T. Happe, *Nat. Chem. Biol.* **2013**, *9*, 607 – 609.
[9] L. Kertess, F. Wittkamp, C. Sommer, J. Esselborn, O. Rudiger, E. J. Reijerse, E. Hofmann, W. Lubitz, M. Winkler, T. Happe, U.-P. Apfel, *Dalton Trans.* **2017**, *46*, 16947 – 16958.
[10] C. Sommer, C. P. Richers, W. Lubitz, T. B. Rauchfuss, E. J. Reijerse, *Angew. Chem. Int. Ed.* **2018**, *57*, 5429 – 5432; *Angew. Chem.* **2018**, *130*, 5527 – 5530.
[11] C. Papini, C. Sommer, L. Pecqueur, D. Pramanik, S. Roy, E. J. Reijerse, F. Wittkamp, V. Artero, W. Lubitz, M. Fontecave, *ACS Catal.* **2019**, *9*, 4495 – 4501.
[12] J. M. Camara, T. B. Rauchfuss, *Nat Chem.* **2012**, *4*, 26 – 30.
[13] Y. Li, T. B. Rauchfuss, *Chem. Rev.* **2016**, *116*, 7043 – 7077.
[14] U.-P. Apfel, C. R. Kowol, Y. Halpin, F. Kloss, J. Kübel, H. Gorls, J. G. Vos, B. K. Keppler, E. Morera, G. Lucente, et al., *J. Inorg. Biochem.* **2009**, *103*, 1236 – 1244.
[15] U.-P. Apfel, C. R. Kowol, E. Morera, H. Gorls, G. Lucente, B. K. Keppler, W. Weigand, *Eur. J. Inorg. Chem.* **2010**, 5079 – 5086.
[16] E. Morera, M. Nalli, F. Pinnen, D. Rossi, G. Lucente, *Bioorg. Med. Chem. Lett.* **2000**, *10*, 1585 – 1588.
[17] A. M. Kluwer, R. Kapre, F. Hartl, M. Lutz, A. L. Spek, A. M. Brouwer, P. W. N. M. van Leeuwen, J. N. H. Reek, *Proc. Natl. Acad. Sci. USA* **2009**, *106*, 10460 – 10465.
[18] L.-C. Song, L.-X. Wang, M.-Y. Tang, C.-G. Li, H.-B. Song, Q.-M. Hu, *Organometallics* **2009**, *28*, 3834 – 3841.
[19] D. Streich, Y. Astuti, M. Orlandi, L. Schwartz, R. Lomoth, L. Hammarstrom, S. Ott, *Chem. Eur. J.* **2010**, *16*, 60 – 63.
[20] F. Wang, W.-G. Wang, X.-J. Wang, H.-Y. Wang, C.-H. Tung, L.-Z. Wu, *Angew. Chem. Int. Ed.* **2011**, *50*, 3193 – 3197; *Angew. Chem.* **2011**, *123*, 3251 – 3255.
[21] M. Wang, L. Chen, X. Li, L. Sun, *Dalton Trans.* **2011**, *40*, 12793.
[22] H.-Y. Wang, G. Si, W.-N. Cao, W.-G. Wang, Z.-J. Li, F. Wang, C.-H. Tung, L.-Z. Wu, *Chem. Commun.* **2011**, *47*, 8406 – 8408.
[23] P. Zhang, M. Wang, Y. Na, X. Li, Y. Jiang, L. Sun, *Dalton Trans.* **2010**, *39*, 1204 – 1206.
[24] X. Li, M. Wang, D. Zheng, K. Han, J. Dong, *Energy Environ. Sci.* **2012**, *5*, 8220-8224.
[25] Y. Na, M. Wang, J. Pan, P. Zhang, B. Akermark, L. Sun, *Inorg. Chem.* **2008**, *47*, 2805 – 2810.
[26] S. Pullen, H. Fei, A. Orthaber, S. M. Cohen, S. Ott, *J. Am. Chem. Soc.* **2013**, *135*, 16997 – 17003.
[27] S. R. Soltau, P. D. Dahlberg, J. Niklas, O. G. Poluektov, K. L. Mulfort, L. M. Utschig, *Chem. Sci.* **2016**, *7*, 7068 – 7078.
[28] R. Goy, L. Bertini, T. Rudolph, S. Lin, M. Schulz, G. Zampella, B. Dietzek, F. H. Schacher, L. De Gioia, K. Sakai, W. Weigand, *Chem. Eur. J.* **2017**, *23*, 334 – 345.
[29] K. Menzel, U.-P. Apfel, N. Wolter, R. Rüger, T. Alpermann, F. Steiniger, D. Gabel, S. Förster, W. Weigand, A. Fahr, *J. Liposome Res.* **2014**, *24*, 59 – 68.
[30] M. Y. Darensbourg, E. J. Lyon, X. Zhao, I. P. Georgakaki, *Proc. Natl. Acad. Sci. USA* **2003**, *100*, 3683 – 3688.
[31] D. W. Mulder, E. M. Shepard, J. E. Meuser, N. Joshi, P. W. King, M. C. Posewitz, J. B. Broderick, J. W. Peters, *Structure* **2011**, *19*, 1038 – 1052.
[32] A. K. Jones, B. R. Lichtenstein, A. Dutta, G. Gordon, P. L. Dutton, *J. Am. Chem. Soc.* **2007**, *129*, 14844 – 14845.
[33] G. Caserta, S. Roy, M. Atta, V. Artero, M. Fontecave, *Curr. Opin. Chem. Biol. Sect. C* **2015**, *25*, 36 – 47.
[34] Y. Sano, A. Onoda, T. Hayashi, *Chem. Commun.* **2011**, *47*, 8229 – 8231.
[35] A. Roy, C. Madden, G. Ghirlanda, *Chem. Commun.* **2012**, *48*, 9816 – 9818.
[36] S. Roy, S. Shinde, G. A. Hamilton, H. E. Hartnett, A. K. Jones, *Eur. J. Inorg. Chem.* **2011**, 1050 – 1055.
[37] A. Onoda, Y. Kihara, K. Fukumoto, Y. Sano, T. Hayashi, *ACS Catal.* **2014**, *4*, 2645 – 2648.
[38] M. E. Wilson, G. M. Whitesides, *J. Am. Chem. Soc.* **1978**, *100*, 306 – 307.
[39] M. Skander, N. Humbert, J. Collot, J. Gradinaru, G. Klein, A. Loosli, J. Sauser, A. Zocchi, F. Gilardoni, T. R. Ward, *J. Am. Chem. Soc.* **2004**, *126*, 14411 – 14418.
[40] G. Klein, N. Humbert, J. Gradinaru, A. Ivanova, F. Gilardoni, U. E. Rusbandi, T. R. Ward, *Angew. Chem. Int. Ed.* **2005**, *44*, 7764 – 7767; *Angew. Chem.* **2005**, *117*, 7942 – 7945.
[41] M. Dürrenberger, T. Heinisch, Y. M. Wilson, T. Rossel, E. Nogueira, L. Knörr, A. Mutschler, K. Kersten, M. J. Zimbron, J. Pierron, et al., *Angew. Chem. Int. Ed.* **2011**, *50*, 3026 – 3029; *Angew. Chem.* **2011**, *123*, 3082 – 3085.
[42] J. M. Zimbron, T. Heinisch, M. Schmid, D. Hamels, E. S. Nogueira, T. Schirmer, T. R. Ward, *J. Am. Chem. Soc.* **2013**, *135*, 5384 – 5388.
[43] V. Köhler, Y. M. Wilson, M. Dürrenberger, D. Ghislieri, E. Churakova, T. Quinto, L. Knörr, D. Häussinger, F. Hollmann, N. J. Turner, T. R. Ward, *Nat. Chem.* **2013**, *5*, 93 – 99.
[44] S. I. Mann, T. Heinisch, A. C. Weitz, M. P. Hendrich, T. R. Ward, A. S. Borovik, *J. Am. Chem. Soc.* **2016**, *138*, 9073 – 9076.

[45] A. Call, C. Casadevall, A. Romero-Rivera, V. Martin-Diaconescu, D. J. Sommer, S. Osuna, G. Ghirlanda, J. Lloret-Fillol, *ACS Catal.* **2019**, *9*, 5837 – 5846.
[46] S. G. Keller, B. Probst, T. Heinisch, R. Alberto, T. R. Ward, *Helv. Chim. Acta* **2018**, *101*, e1800036.
[47] A. Winter, L. Zsolnai, G. Z. Huttner, *Naturforsch. B Anorg. Chem. Org. Chem.* **1982**, *37*, 1430 – 1436.
[48] U.-P. Apfel, Y. Halpin, H. Gorls, J. G. Vos, B. Schweizer, G. Linti, W. Weigand, *Chem. Biodiversity* **2007**, *4*, 2138 – 2148.
[49] F. Zhuanli Shenqing (2017), CN 106632512 a 20170510., n.d.
[50] M. R. Hicks, A. K. Rullay, R. Pedrido, D. H. Crout, T. J. T. Pinheiro, *Synth. Commun.* **2008**, *38*, 3726 – 3750.
[51] J. Brown-McDonald, S. Berg, M. Peralto, C. Works, *Inorg. Chim. Acta* **2009**, *362*, 318 – 324.
[52] M. G. I. Galinato, C. M. Whaley, N. Lehnert, *Inorg. Chem.* **2010**, *49*, 3201 – 3215.
[53] M. L. Singleton, J. H. Reibenspies, M. Y. Darensbourg, *J. Am. Chem. Soc.* **2010**, *132*, 8870 – 8871.
[54] W.-N. Cao, F. Wang, H.-Y. Wang, B. Chen, K. Feng, C.-H. Tung, L.-Z. Wu, *Chem. Commun.* **2012**, *48*, 8081 – 8083.
[55] Y. Na, J. Pan, A. M. Wang, L. Sun, *Inorg. Chem.* **2007**, *46*, 3813 – 3815.
[56] M. Sjödin, S. Styring, B. Akermark, L. Sun, L. Hammarstrom, *J. Am. Chem. Soc.* **2000**, *122*, 3932 – 3936.
[57] H. Murakami, T. Hohsaka, Y. Ashizuka, M. Sisido, *J. Am. Chem. Soc.* **1998**, *120*, 7520 – 7529.
[58] A. Fürstenberg, O. Kel, J. Gradinaru, T. R. Ward, D. Emery, G. Bollot, J. Mareda, E. Vauthey, *ChemPhysChem* **2009**, *10*, 1517 – 1532.
[59] T. R. Ward, *Acc. Chem. Res.* **2011**, *44*, 47 – 57.
[60] T. Heinisch, T. R. Ward, *Acc. Chem. Res.* **2016**, *49*, 1711 – 1721.
[61] M. Dürrenberger, T. R. Ward, *Curr. Opin. Chem. Biol. Sect. C* **2014**, *19*, 99 – 106.
[62] V. Köhler, J. Mao, T. Heinisch, A. Pordea, A. Sardo, Y. M. Wilson, L. Knörr, M. Creus, J.-C. Prost, T. Schirmer, T. R. Ward, *Angew. Chem. Int. Ed.* **2011**, *50*, 10863 – 10866; *Angew. Chem.* **2011**, *123*, 11055 – 11058.
[63] F. Schwizer, V. Köhler, M. Dürrenberger, L. Knörr, T. R. Ward, *ACS Catal.* **2013**, *3*, 1752 – 1755.
[64] T. Heinisch, M. Pellizzoni, M. Dürrenberger, C. E. Tinberg, V. Köhler, J. Klehr, D. Häussinger, D. Baker, T. R. Ward, *J. Am. Chem. Soc.* **2015**, *137*, 10414 – 10419.
[65] C. Lo, M. R. Ringenberg, D. Gnandt, Y. Wilson, T. R. Ward, *Chem. Commun.* **2011**, *47*, 12065 – 12067.
[66] K. K.-W. Lo, W.-K. Hui, D. C.-M. Ng, *J. Am. Chem. Soc.* **2002**, *124*, 9344 – 9345.
[67] K. K.-W. Lo, W.-K. Hui, *Inorg. Chem.* **2005**, *44*, 1992 – 2002.
[68] Z. Otwinowski, W. Minor, *Meth. Enzymol.* **1997**, *276*, 307 – 326.
[69] P. D. Adams, R. W. Grosse Kunstleve, L.-W. Hung, T. R. Ioerger, A. J. McCoy, N. W. Moriarty, R. J. Read, J. C. Sacchettini, N. K. Sauter, T. C. Terwilliger, *Acta Crystallogr. Sect. D* **2002**, *58*, 1948 – 1954.
[70] Collaborative Computational Project, Number 4, *Acta Crystallogr. Sect. D* **1994**, *50*, 760 – 763.
[71] P. Emsley, K. Cowtan, *Acta Crystallogr. Sect. D* **2004**, *60*, 2126 – 2132.

Manuscript received: January 14, 2020
Revised manuscript received: February 24, 2020
Accepted manuscript online: March 22, 2020
Version of record online: ■■ ■■, 0000

Full Paper
doi.org/10.1002/chem.202000204

FULL PAPER

Photochemistry

*A. Roy, M. D. Vaughn, J. Tomlin, G. J. Booher, G. Kodis, C. R. Simmons, J. P. Allen, G. Ghirlanda**

■■ – ■■

Enhanced Photocatalytic Hydrogen Production by Hybrid Streptavidin-Diiron Catalysts

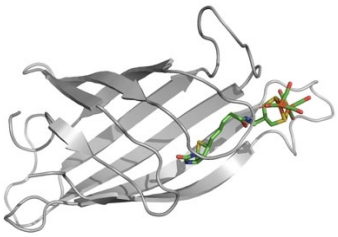

An artificial hydrogenase, StrepH2, was built by incorporating a biotinylated [Fe–Fe] hydrogenase organometallic mimic within streptavidin. Under photocatalytic conditions, the protein-embedded catalyst shows enhanced efficiency and prolonged activity compared to the isolated catalyst (see figure).